N O T I C E

THIS DOCUMENT HAS BEEN REPRODUCED FROM MICROFICHE. ALTHOUGH IT IS RECOGNIZED THAT CERTAIN PORTIONS ARE ILLEGIBLE, IT IS BEING RELEASED IN THE INTEREST OF MAKING AVAILABLE AS MUCH INFORMATION AS POSSIBLE

NASA

Technical Memorandum 83858

SPECTRAL ALBEDOS OF MIDLATITUDE SNOWPACKS

Bhaskar Choudhury

NOVEMBER 1981

National Aeronautics and
Space Administration

Goddard Space Flight Center
Greenbelt, Maryland 20771

SPECTRAL ALBEDOS OF MIDLATITUDE SNOWPACKS

Bhaskar Choudhury

Hydrological Sciences Branch

November 1981

GODDARD SPACE FLIGHT CENTER
Greenbelt, Maryland 20771 (USA)

SPECTRAL ALBEDOS OF MIDLATITUDE SNOWPACKS

Bhaskar Choudhury

Hydrological Sciences Branch
Goddard Space Flight Center
Greenbelt, Maryland 20771 (USA)

ABSTRACT

Spectral albedos of impure-nonhomogeneous snowpacks, typical for midlatitudes, at wavelengths from 400 to 2200 nm are modeled through a numerical solution of the radiative transfer equation in the two-stream approximation. Discrete depth-dependent values of density, grain size and impurity concentration are used to characterize the snowpacks. The model is for diffuse incident radiation, and the numerical method is based on doubling and invariant imbedding. The effect of soot impurities on snowpack albedos is illustrated: when a snowpack is semi-infinite (thickness of ten centimeters or more), soot reduces the albedos at visible wavelengths; however, for smaller snowpack thicknesses soot may increase the albedos at visible wavelengths. By adjusting soot content and snow grain size, good quantitative agreement with some observations at the Cascade Mountains (Washington) and at Point Barrow (Alaska) are obtained; however, the model grain sizes are found to be fifty to four hundred percent larger than the measured values. For satellite snowcover observations, a model for effective albedo of partially snow-covered areas is developed and compared with some NOAA-2 observations of the southeastern United States.

SPECTRAL ALBEDOS OF MIDLATITUDE SNOWPACKS

INTRODUCTION

In mid-latitudes (30° - 60°), snowpacks accentuate their importance as a valuable water resource for consumptive, industrial and agricultural use, and in flood control due to spring snowmelt runoff. Hydrologic importance of snowpacks, for example, in the Salt-Verde watershed in Arizona, and in the Sierra Nevada and the Cascade Range has been well documented (Rango, 1975) The appearance and disappearance (except may be on high mountains) of snow at mid-latitudes creates a climatically sensitive transition zone because snow exerts considerable influence on weather and climate through numerous feedback processes (Hahn and Shukla, 1976; Kukla, 1981; Reiter and Reiter, 1981). The snow data (e.g., areal coverage, depth, liquid water equivalent) from isolated weather stations are of limited use for hydrologic and climatic studies because they are point observations and extrapolation for areally representative values would be questionable. Attempts are being made to obtain areally representative (including global) snow data, through remote sensing via visible, infrared and microwave radiometers (cf. McGinnis et al., 1975; Foster et al., 1980; Matson and Wiesnet, 1981).

Mid-latitude snowpacks are shallow (depth generally less than one meter except in high mountain environments), non-homogeneous (temperature gradient and melt-freeze metamorphisms and deposition of new snow on top of old metamorphosed snow) and impure (deposition of dust and soot from the atmosphere and scavenging of aerosols by the falling snow crystals). The objective of this paper is to formulate and study a model for spectral shortwave albedo of non-homogeneous shallow snowpacks contaminated with impurities. Although incident radiation is assumed to be diffuse, the calculated albedos would be representative of those for the clear sky conditions at the solar elevation of about 35° (Wiscombe and Warren, 1980), i.e., about noon during the spring snow-melt period.

In the next section the model is formulated in terms of a numerical solution of the radiative transfer equation. Illustrative results and comparisons with field and satellite observations are

then given. Some basic understanding of the radiative transfer process within a snowpack is gained through comparison with field observations, although interpretation of satellite data required addressing additional issues. Previous studies (Warren and Wiscombe, 1980; Dozier et al., 1981; Choudhury et al., 1981) had concluded that absorbing impurities like soot would lower the visible albedo of a snowpack. The present calculations show that this effect of soot is not always true; when a snowpack is not semi-infinite (i.e., thickness less than 100 mm, see Wiscombe and Warren (1980)) the visible albedo of an impure snowpack could actually be higher than that for pure snow. Comparison with satellite observations indicate that snow depth may be inferred from narrow band sensor data in the visible region, and this sensitivity to snow depth appears because the fractional snow covered area which determines the brightness of picture elements depends upon snow depth.

FORMULATION FOR FIELD OBSERVATIONS

A snowpack is a delicate lattice whose nuclei are ice grains of various shape and size. The impurities could be attached to or imbedded in the ice grains or ligatures. In albedo studies (Bohren and Barkstrom, 1974; Choudhury and Chang, 1979; Wiscombe and Warren, 1980), a homogeneous snowpack of finite thickness has been modeled as isolated spherical particles which scatter and absorb the radiation incident on top of the snowpack. (An exception being Dunkle and Bevans (1956), who modeled the ice grains as facets.) The effect of absorbing impurities has been studied quantitatively within this schematic model of a snowpack (Warren and Wiscombe, 1980; Choudhury et al., 1981). As an extension, a nonhomogeneous snowpack will be modeled as homogeneous layers (Fig. 1), i.e., the model nonhomogeneous snowpack consists of layers which have characteristic values of density, grain size and impurity content.

Within the above schematic representation of a nonhomogeneous snowpack, the albedo will be calculated through the two-stream approximation (Choudhury and Chang, 1979; Choudhury et al., 1981) of the radiative transfer equation. In this approximation, the radiation within the snowpack is divided into upwelling (F_-) and downwelling (F_+) fluxes, which satisfy the equations

$$\frac{dF_+}{dx} = \sqrt{3}\gamma_e \left[-F_+ + \frac{\omega}{2}(1+g)F_+ + \frac{\omega}{2}(1-g)F_- \right] \quad (1a)$$

$$-\frac{dF_-}{dx} = \sqrt{3}\gamma_e \left[-F_- + \frac{\omega}{2}(1+g)F_- + \frac{\omega}{2}(1-g)F_+ \right] \quad (1b)$$

where the radiative transfer parameters γ_e, ω, and g are called the extinction coefficient, the single scattering albedo and the asymmetry parameter of the scattering phase function. These radiative transfer parameters vary with the wavelength and are functions of depth, x, through their dependence on the physical properties of the snowpack, namely, grain size, density and impurity concentration. Calculation of the radiative transfer parameters from snowpack physical properties will be discussed before presenting the method of solution for eqns.(1).

Since ice grains of a snowpack are two or more orders of magnitude larger than the wavelength, scattering by individual ice grains is strongly in the forward direction (the well known diffraction component). In considering the radiative transfer process in powdered media, Hapke (1981) scrutinized the definition of the diffraction component as to whether this component should be treated as a part of the scattered radiation. As the inter-particle separation decreases, the particles enter into the geometric shadow of neighbouring particles, and Hapke (1981) concludes that when shadowing occurs the diffracted light must be treated as being indistinguishable from unscattered incident radiation. The condition for neglecting diffraction component as being a part of the scattered radiation is, for ice particles, given by (Hapke, 1981)

$$\left(\frac{\rho_s}{\rho_i}\right)^{-1/3} \lesssim 0.94 \left(\frac{r}{\lambda}\right)^{1/3} \quad (2)$$

where ρ_i is density of ice, ρ_s is snow density, r is the grain radius and λ is the wavelength. The condition (2) implies that for natural snowpacks the diffracted radiation should almost always be neglected in calculating the radiative transfer parameters in eqns.(1).

Noting that the extinction cross-section for particles two or more orders of magnitude larger than the wavelength can be taken as πr^2 when the diffraction component is excluded, the extinction

coefficient is given by (cf., Choudhury and Chang, 1979)

$$\gamma_e = \frac{3}{4r} \left(\frac{\rho_s}{\rho_i}\right) \tag{3}$$

where ρ_i is the density of ice (917 kg m^{-3}).

The single scattering albedo is the ratio of scattering and extinction cross-sections. This albedo inclusive and exclusive of the diffraction component, Ω and ω respectively, are related as (Van de Hulst, 1962)

$$\Omega = \tfrac{1}{2} (1 + \omega) \tag{4}$$

In previous studies by the author and his co-workers (cf. Choudhury et al., 1981) the following equation obtained from Irvine and Pollack (1968) was used,

$$\omega \quad \exp (-1.67\ kr) \tag{5}$$

where k is the spectral absorption coefficient of the sphere. This equation for ω has the shortcoming that for very large spheres ($r \to \infty$), ω tends to zero instead of approaching the correct value $\omega \simeq 0.066$ (Irvine, 1965). This shortcoming arises because eqn.(5) neglects the rays reflected by the surface (Irvine and Pollack, 1968). Although the error in calculating Ω with this shortcoming was found to be generally less than 5%, following Thomas (1952), the equation for ω chosen for this study is

$$\omega = 0.066 + 0.934 \exp (-1.75\ kr) \tag{6}$$

A comparison of Ω obtained from (4) and (6) with the Mie theory results of Wiscombe and Warren (1980) is given in Table 1.

The asymmetry parameter, G, inclusive of the diffraction component is related to the corresponding parameter, g, excluding the diffraction component as (Van de Hulst, 1962)

$$G = \frac{1 + \omega g}{1 + \omega} \tag{7}$$

Using the following parameterized equation for G (Choudhury et al., 1981),

$$G = 0.886\,\omega + 0.978\,(1 - \omega) \tag{8}$$

one obtains

$$g = 0.886 - 0.092\,\omega - \frac{0.022}{\omega} \tag{9}$$

A comparison of eqn. (8) with the Mie theory results of Wiscombe and Warren (1980) is given in Table 2. Computationally, eqns. (6) and (9) are at least an order of magnitude less time consuming than the Mie theory.

Although previous studies (e.g., Choudhury and Chang, 1979; Wiscombe and Warren, 1980; Warren and Wiscombe, 1980; Choudhury et al., 1981) on snow albedo had included the diffraction component in calculating the radiative transfer parameters, it is shown in the Appendix that the calculated albedos from Choudhury and Chang's (1979) model remain unchanged when the diffraction component is excluded, as it is done here.

For pure snow, the absorption coefficients of ice from Grenfell and Perovich (1981) (from 400 to 1400 nm) and Hobbs (1974) are used in eqn.(6). For soot contaminated snow, an effective absorption coefficient for soot-ice mixture is calculated by averaging the absorption coefficients of ice and soot by the corresponding volume fractions (see eqn.4 in Choudhury et al., 1981). The characteristics assigned to the soot particles are density 1130 kg m^{-3}, imaginary part of the refractive index 0.5 and particle volume 3.93×10^{-21} m^3. The density and the refractive index of soot are for the assumed porosity of 50% (Chylek et al., 1981). (The results of Choudhury et al. (1981) were based on a higher value of soot density, 2260 kg m^{-3}, which actually corresponds to pure carbon. The porosity of soot is generally between 30 to 50%.)

For homogeneous snowpacks (i.e., ρ_s, r and γ_e are independent of depth x) the solution of eqns.(1) can be obtained analytically (Choudhury and Chang, 1979). A numerical method, however, is needed for nonhomogeneous snowpacks. The numerical method used in this paper is based on doubling and invariant imbedding (Twomey et al., 1966 and Grant and Hunt, 1969). Instead of discussing the numerical method in general terms, the basic steps in the algorithm implementation will be outlined.

Step 1: Initialization

Divide snowpack into NL homogeneous layers (Fig. 1) and prescribe the layer characteristics,

$$\text{Thickness}: \Delta x_1, \Delta x_2, \Delta x_3, \ldots\ldots, \Delta x_{NL}$$

$$\text{Grain Radius}: r_1, r_2, r_3, \ldots\ldots\ldots, r_{NL}$$

$$\text{Density}: \rho_1, \rho_2, \rho_3, \ldots\ldots\ldots, \rho_{NL}$$

$$\text{Soot Content}: S_1, S_2, S_3, \ldots\ldots\ldots, S_{NL}$$

After initialization execute the following steps for *each* wavelength.

Step 2: Parameter Calculation

Calculate the effective absorption coefficient (as discussed previously) and

$$\text{Single Scattering Albedo}: \omega_1, \omega_2, \omega_3, \ldots\ldots\ldots, \omega_{NL}$$

$$\text{Extinction Coefficient}: \gamma_1, \gamma_2, \gamma_3, \ldots\ldots\ldots, \gamma_{NL}$$

$$\text{Asymmetry Parameter}: g_1, g_2, g_3, \ldots\ldots\ldots, g_{NL}$$

Step 3: Doubling

For each layer J (J = 1, 2, . . . NL), find an integer N such that

$$\gamma_J \left(\frac{\Delta x_J}{2^N} \right) < 10^{-4} \qquad (10)$$

Calculate $T_N(J)$ and $R_N(J)$ through the following recurrence relations ($k = 1, 2, \ldots N$)

$$T_k(J) = \frac{T^2_{k-1}(J)}{1 - R^2_{k-1}(J)} \tag{11}$$

$$R_k(J) = R_{k-1}(J) + \frac{T^2_{k-1}(J)\, R_{k-1}(J)}{1 - R^2_{k-1}(J)} \tag{12}$$

with the starting relations

$$T_0(J) = 1 - \sqrt{3}\,\gamma_J \left[1 - \tfrac{1}{2}\omega_J (1 + g_J)\right] \frac{\Delta x_J}{2^N} \tag{13}$$

$$R_0(J) = \frac{\sqrt{3}}{2}\,\gamma_J\, \omega_J (1 - g_J) \frac{\Delta x_J}{2^N} \tag{14}$$

Step 4: Invariant Imbedding

Using NL values of $T_N(J)$ and $R_N(J)$ ($J = 1, 2, \ldots, NL$), execute the recurrence relations ($L = 1, 2, \ldots, NL - 1$)

$$\tilde{T}(L + 1) = \frac{T_N(L + 1)\, \tilde{T}(L)}{1 - \tilde{R}(L)\, R_N(L + 1)} \tag{15}$$

$$\tilde{R}(L + 1) = \tilde{R}(L) + \frac{T^2_N(L + 1)\, \tilde{R}(L)}{1 - \tilde{R}(L)\, R_N(L + 1)} \tag{16}$$

with the starting relations

$$\tilde{T}(1) = T_N(1) \tag{17}$$

$$\tilde{R}(1) = R_N(1) \tag{18}$$

Step 5: Spectral Albedo of Snow-Soil System

If α is the spectral albedo of underlying soil, then the spectral albedo (A) of the snow-soil system is

$$A = \tilde{R}(NL) + \frac{\tilde{T}^2(NL)\, \alpha}{1 - \alpha\, R(NL)} \tag{19}$$

Spectral albedo of wet clay soil (Lulla, 1980) used in the calculation is shown in Fig. 2.

When the snow is crusted, one needs to consider the reflection due to the dielectric discontinuity at top and bottom crust surfaces and attenuation within the crust layer. If the crust layer is assumed to be homogeneous (i.e., void of any trapped impurities, air bubbles, etc.) with smooth surfaces (i.e., neglecting corrugation due to fused ice grains) then one can use Fresnel equations to calculate the reflectivities (Jerlov, 1976; Lyzenga, 1977), and an effective transmission coefficient (cf., Hottel et al., 1968) for the layer. An equation analogous to (19) is obtained for crusted snow

$$A' = R_{ai} + T_c^2 \left\{ \frac{A}{1 - R_{ai} A} \right\} \tag{20}$$

where A is defined in eqn. 19, R_{ai} is Fresnel reflectivity at the air-ice interface for diffuse radiation (≈ 0.066; Jerlov, 1976) and T_c is effective transmission coefficient of crust layer for diffuse radiation, given by

$$T_c = (1 - R_{ai})(1 - R_{ia})\tau \left\{ \frac{1}{1 - (\tau R_{ia})^2} \right\} \tag{21}$$

where R_{ia} is Fresnel reflectivity at the ice-air interface for diffuse radiation (≈ 0.475; Lyzenga, 1977) and τ is the transmission function of the crust layer due to absorption,

$$\tau = \exp(-\sqrt{3}\, k\, d) \tag{22}$$

k being the absorption coefficient and d the thickness of the crust layer.

If the physical characteristics of a snowpack are known, the theory outlined above can be used to calculate its spectral albedos. In remote sensing via air- and satellite-borne sensors, the required physical characteristics are not generally known, and in fact a thrust of remote sensing is to infer the physical characteristics (e.g., the liquid water equivalent) from the sensor data. Also, high altitude observations would generally give the reflectivity of an area which is not uniformly covered with snow. The above theory needs to be amended for reflectively heterogeneous scenes.

In the next section, the above theory will be compared with field observations (uniformly snow-covered area). The understanding of the radiative transfer process gained through this comparison will be used together with some ancillary data and an extension of the model to reflectively heterogeneous scenes for comparing with satellite observations.

ILLUSTRATIVE RESULTS AND COMPARISONS

Spectral albedo of deep soot-contaminated snowcover was studied previously by Choudhury et al. (1981). The study showed that the effect of soot is to *lower* the spectral albedo in visible and in near-infrared up to about 1100 nm. Furthermore, for the same weight fraction of soot, the reduction in albedo for a coarse grained snow was shown to be higher compared to a fine grained snow. Whereas the calculated spectral albedos for pure snow were generally higher than observations, the study substantiated Warren and Wiscombe's (1980) work in providing a qualitative explanation for observed albedos. Choudhury et al. (1981), however, found some difficulty in matching concurrent observations of spectral albedos and flux extinction coefficients which they ascribed to be due to either approximations in the model or inaccuracies in the observations. Since the present model is essentially a modification of Choudhury et al. (1981) model to incorporate layered nonhomogenities, the present model would not materially alter the conclusions of Choudhury et al. when snow is deep and homogeneous. Choudhury et al. showed a comparison with the observations of Grenfell (1982). This comparison will be shown again, and will be complemented by comparisons with the observations of Grenfell et al. (1981) because the soot density used by Choudhury et al. (namely, 2260 kg m^{-3}) was a factor of two larger than the one used in this study. (I have stated previously that the density 2260 kg m^{-3} is for solid carbon, and Warren and Wiscombe (1980) had correctly noted that soot being a porous carbon should have a lower density.) Some differences with Choudhury et al. also arise because the expression for the single scattering albedo and the absorption coefficient of ice in the spectral range 400 to 1400 nm are slightly different in these two studies (see discussion in FORMULATION).

Comparison between observed (Grenfell, 1982; Grenfell et al., 1981) and calculated albedos for deep snowcovers are shown in Figs. 3(A, B, C), and observed and model physical parameters are given in Table 3. Observations in Fig. 3A are for new snow with ambient air temperature of 0°C, while for Figs. 3B and 3C snow is old and ambient air temperatures are, respectively, -11°C and +13°C. All three figures show calculated albedos for pure (dotted curve) and soot contaminated (solid line) snow, and it is seen that without absorbing impurities the calculated albedo in the spectral range 400 to about 1000 nm are several percent higher than observations. In the spectral range 1500 to 2200 nm, the calculated albedos are generally 3 to 10 percent lower than observations, which could be due to uncertainties in the absorption coefficient of ice (cf., Wiscombe and Warren, 1980). The physical parameters given in Table 3 show that as the observed grain size increases, so does the model grain size. However, the model grain sizes are 1.5 to 2.5 times larger than the observed values.

Model calculations assume spherical grains, whereas natural snow grains are rarely spherical. Since model calculation for nonspherical particles is more difficult than for spherical particles, it would be useful to find a measurable physical characteristic (e.g., $(\text{volume})^{1/3}$, $(\text{surface area})^{1/2}$) which could be directly related to the model grain size (cf., O'Brien and Koh, 1981). A further point worth noting in Table 3 is the amount of soot needed to match the observations in Figs. 3A and 3C which are from the same area (Cascade Mountains, Washington); the new snow in Fig. 3A contains, according to the model, about six times more soot than old snow in Fig. 3C. Soot contamination in new snow would most likely be due to scavenging of atmospheric aerosols by the falling snow crystals. With aging one would expect the concentration of soot to increase due to fallout. Table 3, however, shows just the opposite trend for soot, although a substantial amount of dust was observed for Fig. 3C. One way to reconcile this discrepancy would be to postulate that snow-melt water rinses the micron size soot particles but not the larger dust particles. For matching the observations in Fig. 3B, Choudhury et al. (1981) used 0.5 ppmw (parts per million by weight) of soot, and the reason for a lower amount of soot in Table 3 is primarily the lower soot density used in this study.

Comparison with observed albedos for a two-layer deep snowpack is shown in Fig. 4, and the observed and model physical parameters are given in Table 3. Snow in the surface 30 mm is less than two days old, and the model grain size is somewhat unrealistically larger by about a factor of four than the observed size. Note also that soot in the surface layer *increases* the albedo up to about 1000 nm. Fig. 5(A, B) further illustrates the effect of soot in shallow (less than a few centimeters deep) snowpacks. That absorbing impurities would *increase* the albedo when a snowpack is only a few centimeters deep is understandable. Choudhury et al. (1981) showed that the flux extinction coefficient, which determines whether a snowpack is semi-infinite at any wavelength, increases with soot content. The albedo of a few centimeters deep pure snow is lower in the visible because the incident radiation penetrates the snow layer, and thus is able to 'see' a comparatively lower reflecting underlying soil (or metamorphosed snow). Soot increases the extinction coefficient and thus making a snow layer appear semi-infinite for thicknesses smaller than it would be for pure snow. With a thin (a few centimeters) layer of pure snow on a black surface, an interesting experiment would be to confirm that the albedo in the visible region to increase first and then decrease as absorbing impurities are added to the snowpack. An illustration of this interesting soot dependence of albedos is given in Fig. 6.

Above comparisons showed that spectral albedos for uniformly snow covered areas can be matched if the model grain size and soot content are treated as adjustable parameters, and that fairly new snow contains 'substantial' amount of absorbing impurities. In many observations by aircraft and satellite borne sensors the observed areas are not uniformly snow covered. Noting the relevance of satellite observed snow data in hydrologic and climatic studies, a semi-empirical analysis of data from the Very High Resolution Radiometer (VHRR) on board the NOAA-2 satellite will be given.

A linear model for spectral albedo of a reflectively heterogeneous scene can be written as

$$A_{eff} = \sum_{j=1}^{n} f_j \, A_j \qquad (23)$$

where n is the number of components whose fractional areas visible to the sensor are f_j and albedos A_j. (Note $\sum_{j=1}^{n} f_j = 1$.) For a two-component scene (snow and vegetation), the equation would be

$$A_{eff} = f A_{snow} + (1 - f) A_{veg} \qquad (24)$$

where f is the fractional snow covered area visible to the sensor.

Satellite observations are the bidirectional reflectance of the earth-atmosphere system generally in narrow spectral bands. The albedos calculated here consider fluxes rather than intensities; however, O'Brien and Munis' (1975) study shows a strong resemblance between the bidirectional reflectance and the albedo. Even with such resemblance, a direct quantitative comparison between the present model and the satellite observations can not be made because of spectral absorption and scattering by atmospheric molecules and aerosols. Dozier et al., (1981) have attempted to include the atmospheric effects, but a simpler approach of calculating the 'relative reflectance' was followed by McGinnis et al. (1975). for the VHRR data. A quantity equivalent to the relative reflectance will be the effective albedo normalized by its maximum value. This normalization would minimize the atmospheric effects.

For the VHRR sensor, bandwidth 0.6 - 0.7 μm, $A_{veg} \approx 0.07$ (Tucker, 1979; Kondratyev et al., 1981). The snow albedo does vary with snow thickness but, if comparison in Fig. 3A and illustration in Fig. 5A are any guide, the fairly new snow observed by McGinnis et al. contained enough impurities to make two or three centimeters deep snow behave optically semi-infinite. From Fig. 3A we get $A_{snow} \approx 0.95$. If the fractional snow covered area is known then eqn.(24) can be used to compute the effective albedo.

The fractional snow-covered area that would be visible to a sensor depends, apart from sensor angle, on sun altitude, snow depth and surface features (e.g., canopy type, architecture and spac-

ing). With low sun altitude, the incident rays may get largely intercepted by the canopies, leaving the snowcovered ground mostly in shadows. Clearly, tall coniferous trees are more effective in 'hiding' the snow from the sensor view than coniferous shrubs and deciduous trees.

In rugged terrains and low density coniferous forrests, the pixel brightness may increase in late winter or early spring (before snow melt) due solely to higher solar altitudes. With increasing snow depth, furrows of a farm, scattered boulders, grass and other small plants and shrubs get covered with snow; only the taller plants protrude. The fractional snowcovered area will, therefore, increase as the snow depth increases, approaching the limiting value of 1.0 only if all objects within the pixel are covered with snow.

A formal theory for fractional snow-covered area should certainly consider statistical or deterministic information about surface land features (e.g., height distribution and density of vegetation) within the pixel area. Instead of developing and verifying such a theory in this paper, I have used aircraft albedo observations of Kung et al. (1964) to calculate f. A brief discussion of Kung et al. experiment and calculation of f follows.

A pair of upward and downward looking Kipp and Zonen solarimeters on board a Cessna 310 aircraft were used by Kung et al. (1964) to study the *spectrally integrated albedo* over North America. The ratio of albedos for snow-covered and non snow-covered farm, mixed farm and forest, and forest areas in Wisconsin with a ground resolution of 21 x 70 meters is plotted as a function of snow depth in Kung et al. (1964). To analyze these plotted data, a linear model for albedo would be

$$\frac{<A_{eff}>}{<A_{veg}>} = f \frac{<A_{snow}>}{<A_{veg}>} + (1 - f) \qquad (25)$$

where the angular brackets are used to denote spectrally averaged values.

To calculate the fractional snow-covered area (f), it is thought that mixed farm and forest land data of Kung et al. would be somewhat morphologically compatible with 32 x 32 km squares VHRR data of McGinnis et al. (1975) for southeastern United States. The pertinent data are shown in Fig. 7, and expressed parametrically as

$$\frac{<A_{eff}>}{<A_{veg}>} = \frac{60 + 3.6\,x}{60 + x} \tag{26}$$

where x is the snow depth (in mm). From eqns. (25) and (26) one can calculate f if snow and vegetation albedos are known. Kung et al. give the mean $<A_{veg}>$ for woody farm lands in Wisconsin as 0.144. Snow albedo is highly variable, and the factors affecting this albedo are metamorphism, impurity contamination and snow depth. The snow in Kung et al. observations was at least two days old and, if the comparison shown in Fig. 3A is any guide, contains enough impurities to stipulate that a snow layer only two or three centimeters deep would be effectively semi-infinite. If in Fig. 7 the largest ratio, 5.4 is assumed to be for f=1 (i.e., uniform snow cover) then the corresponding snow albedo is 0.778. The data in Fig. 7 spans the entire snow season, and a snow albedo 0.778 is not totally unrealistic mean value for this data. Taking $<A_{snow}> / <A_{veg}> = 5.4$, the fractional snow-covered area is obtained as (from Eqns. 25 and 26)

$$f = \frac{0.6\,x}{60 + x} \tag{27}$$

From eqns. (24) and (27), the equation for pixel brightness (albedo) is

$$A_{eff} = \frac{4.2 + 0.6\,x}{60 + x} \tag{28}$$

The effective albedo normalized to its value for x = 650 mm (i.e., $A_{eff} = 0.56$) calculated from eqn. (28) is shown in Fig. 8 together with the NOAA-2 observations of McGinnis et al. (1975). The calculated trend is in qualitative agreement with the observations; for a given snow depth, the calculated brightness value being somewhat higher than the observed mean value. McGinnis et al., however, had noted that the snow depth values that were associated with the

brightness values may have been overestimated. The effect of associating a smaller snow depth value with the brightnesses would be to shift the data points to the left and, if done, the agreement with calculation will improve.

Note that the dependence of pixel brightness on snow depth is solely due to the dependence of the fractional snow-covered area on snow depth. Eqn. (27) for the fractional snow-covered area, obtained using Kung et al. (1964) data, implicitly includes sun angle and vegetation morphology dependencies that was prevalent in Wisconsin, and its application to the NOAA-2 data for southeastern United States has not been rigorously justified. Comparison shown in Fig. 7 should, therefore, be tentative. If satellite observations are to be used to estimate snow depth, *ab initio* modeling of the fractional snow-covered area seems warranted.

SUMMARY

Midlatitude snowpacks are a valuable water resource, and being in a climatic transition zone exerts considerable influence on weather and climate through numerous feedback processes. These snowpacks are generally nonhomogeneous and contain impurities, and an understanding of their spectral albedos is needed in energy balance calculations and remote sensing via visible and near-infrared radiometers.

By characterizing a snowpack with depth-dependent density, grain size and impurity concentration, spectral albedos from 400 to 2200 nm are modeled through a numerical solution of the radiative transfer equation. The model is for diffuse incident radiation, and the numerical method is based on doubling and invariant imbedding. The radiative transfer parameters (extinction coefficient, single scattering albedo and asymmetry parameter of the phase function), which describe scattering and absorption by the snow grains, are expressed analytically in terms of model grain size, measurable density and impurity content of the snowpack. The diffraction component of the scattered radiation is excluded in calculating the radiative transfer parameters to account for smaller inter-particle (grains) separation in snowpacks as compared to that in clouds or in the atmosphere.

Model calculations show that when a snowpack is several centimeters deep, soot impurities reduces the albedos up to about 1000 nm; however, for a few centimeters deep snowpacks, soot impurities may increase the albedo as compared to that for pure snow. Good quantitative agreement with some observed spectral albedos at the Cascade Mountains (Washington) and Point Barrow (Alaska) are shown, but the model grain sizes are larger than the measured values. The comparison points towards a better understanding of the meaning of the model grain size, as it is related to measurable dimensions of snow grains.

For interpreting satellite snow-cover observations, a model for effective albedo of partially snow-covered areas is developed. An equation for the fractional snow-covered area, dependent upon the snowpack thickness, is obtained by analyzing a set of aircraft albedo observations. The predictions of the effective albedo model are in qualitative agreement with the NOAA-2 satellite data for the southeastern United States. It is concluded that remote sensing of snow depth using satellite data should address the question of fractional snow-covered area through *ab initio* modeling.

APPENDIX: INVARIANCE OF CHOUDHURY-CHANG (1979) MODEL WITH RESPECT TO THE DIFFRACTION COMPONENT

The aim of this appendix is to show that spectral albedo and asymptotic flux extinction coefficients of snow obtained by Choudhury and Chang (1979) for diffuse incident radiation remain invariant with respect of inclusion or exclusion of the diffraction component in the radiative transfer parameters.

Using the notation of this paper (FORMULATION) for the radiative transfer parameters, the spectral albedo (A) and the asymptotic flux extinction coefficient (ϕ) obtained by Choudhury and Chang are

$$A = \frac{(\alpha A_{\infty} - 1) A_{\infty} + (A_{\infty} - \alpha) e^{-2\phi h}}{(\alpha A_{\infty} - 1) + A_{\infty} (A_{\infty} - \alpha) e^{-2\phi h}} \qquad \text{(A-1)}$$

$$\phi = \Sigma_{ext} N [3 (1 - \Omega) (1 - \Omega G)]^{1/2} \qquad \text{(A-2)}$$

α is soil albedo, h is snowpack thickness, Σ_{ext} is the extinction cross-section inclusive of diffraction ($2\pi r^2$), N is the number density of snow grains and A_{∞} is the spectral albedo for infinitely thick snowpack ($h \to \infty$), given by

$$A_{\infty} = 1 - \frac{2(1 - \Omega)^{1/2}}{(1 - \Omega)^{1/2} + (1 - \Omega G)^{1/2}} \qquad \text{(A-3)}$$

The radiative transfer parameters Ω and G inclusive of the diffraction component are related to the corresponding parameters excluding the diffraction component ω and g by relations (Van de Hulst, 1962)

$$G = \frac{1 + \omega g}{1 + \omega} \qquad \text{(A-4)}$$

$$\Omega = \tfrac{1}{2} (1 + \omega) \qquad \text{(A-5)}$$

One can easily verify that eqn. (A-3) for A_{∞} remains invariant when eqns. (A-4) and (A-5) are substituted in this equation. The eqn. (A-2) can also be seen to remain invariant when (A-4) and (A-5) are used, remembering that the extinction cross-section (σ_{ext}) when the diffraction component is excluded is ½ Σ_{ext}.

Thus the spectral albedos and the asymptotic flux extinction coefficients calculated from Choudhury and Chang's model will be identical to those calculated excluding the diffraction component.

REFERENCES

Bohren, C. F. and Barkstrom, B. R. (1974), Theory of the optical properties of snow, J. Geophys. Res., 79: 4527-4535.

Choudhury, B. J. and Chang, A. T. C. (1979), Two-stream theory of reflectance of snow, IEEE Trans. Geosci. Electronics, GE-17: 53-68.

Choudhury, B. J., Mo, T., Wang, J. R. and Chang, A. T. C. (1981), Albedo and flux extinction coefficients of impure snow for diffuse short-wave radiation, Cold Regions Sci. Technol., 5:

Chylek, P., Ramaswamy, V., Cheng, R. and Pinnick, R. G. (1981), Optical properties and mass concentration of carbonaceous smokes, Appl. Opt., 20: 2980-2985.

Dozier, J., Schneider, S. R. and McGinnis, D. F. (1981), Effect of grain size and snowpack water equivalence on visible and near-infrared satellite observations of snow, Water Resour. Res., 17: 1213-1221.

Dunkle, R. V. and Bevans, J. T. (1956), An approximate analysis of the solar reflectance and transmittance of a snow cover, J. Meteorol., 13: 212-216.

Foster, J. L., Rango, A., Hall, D. K., Chang, A. T. C., Allison, L. J. and Diesen, B. C. (1980), Snowpack monitoring in North America and Eurasia using passive microwave satellite data, Remote Sens. Environ., 10: 285-298.

Grant, I. P. and Hunt, G. E. (1969), Discrete space theory of radiative transfer, Proc. Roy. Soc. (Lon.), A313: 199-216.

Grenfell, T. C. (1982), An infrared scanning photometer for field measurements of spectral albedo and irradiance under polar conditions, J. Glaciol.

Grenfell, T. C. and Perovich, D. K. (1981), Radiation absorption coefficients of polycrystalline ice from 400 - 1400 nm, J. Geophys. Res., 86: 7447-7450.

Grenfell, T. C., Perovich, D. K. and Ogren, J. A. (1981), Spectral albedos of an alpine snowpack, Cold Regions Sci. Technol., 4: 121-127.

Hahn, D. G. and Shukla, J. (1976), An apparent relationship between Eurasian snow cover and Indian monsoon rainfall, J. Atmos. Sci., 33: 2461-2462.

Hapke, B. (1981), Bidirectional reflectance spectroscopy, I: theory, J. Geophys. Res., 86: 3039-3054.

Hobbs, P. V. (1974), Ice Physics, Clarendon Press, Oxford.

Hottel, H. C., Sarofim, A. F., Evans, L. B. and Vasalos, I. A. (1968), Radiative transfer in anisotropically scattering media: allowance for Fresnel reflection at the boundaries, Trans. ASME, J. Heat Trans., 90: 56-62.

Irvine, W. M. (1965), Light scattering by spherical particles: radiation pressure, asymmetry factor, and extinction cross section, J. Opt. Soc. Am., 55: 16-59.

Irvine, W. M. and Pollack, J. B. (1968), Infrared optical properties of water and ice spheres, Icarus, 8: 324-360.

Jerlov, N. G. (1976), Marine Optics, p. 75, Elsevier Scientific Publication Company, New York.

Kondratyev, K. Ya., Korzov, V. I. Mukhenberg, V. V. and Dyachenko, L. N. (1981), The shortwave albedo and the surface emissivity, GARP Study Conf. on Land Surface Processes in Atmos. Gen. Cir. Models (unpublished preprints).

Kukla, G. (1981), Climatic role of snow covers, IAHS Publ. no. 131: 79-107.

Kung, E. C., Bryson, R. A. and Lenschow, D. H. (1964), Study of a continental surface albedo on the basis of flight measurements and structure of the Earth's surface cover over North America, Mon. Weather Rev., 92: 543-564.

Lulla, K. (1980), Remote sensing and soil studies: a brief review, Rem. Sens. Quarterly, 2: 4-20.

Lyzenga, D. R. (1977), Reflectance of a flat ocean in the limit of zero water depth, Appl. Opt., 16: 282-283.

Matson, M. and Wiesnet, D. R. (1981), New data base for climatic studies, Nature, 289: 451-456.

McGinnis, D. F., Pritchard, J. A. and Wiesnet, D. R. (1975), Determination of snow depth and snow extent from NOAA-2 Satellite very high resolution radiometer data, Water Resour. Res., 11: 897-902.

O'Brien, H. W. and Munis, R. H. (1975), Red and near-infrared spectral reflectance of snow, in: A. Rango (Ed.) Operational Applications of Satellite Snowcover Observations, NASA-SP-391.

O'Brien, H. W. and Koh, G. (1981), Near-infrared reflectance of snow-covered substrates, U.S. Army Cold Regions Res. Eng. Lab. (preprint).

Rango, A. (1975), Operational applications of satellite snowcover observations, National Aeronautics and Space Administration, NASA-SP-391.

Reiter, E. R. and Reiter, G. J. (1981), Tibet the last frontier, Bull. Am. Met. Soc., 62: 4-13.

Thomas, P. H. (1952), Absorption and scattering of radiation by water sprays of large drops, Brit. J. Appl. Phys., 3: 385-393.

Tucker, C. J. (1979), Red and photographic infrared linear combinations for monitoring vegetation, Remote Sens. Environ., 8: 127-150.

Twomey, S., Jocobowitz, H. and Howell, H. B. (1966), Matrix method for multiple-scattering problems, J. Atmos. Sci., 23: 289-296.

Van de Hulst, H. C. (1962), Light Scattering by Small Particles, p. 225, John Wiley, New York.

Warren, S. G. and Wiscombe, W. J. (1980), A model for the spectral albedo of snow II: snow containing atmospheric aerosols, J. Atmos. Sci., 37: 2712-2733.

Wiscombe, W. J. and Warren, S. G. (1980), A model for the spectral albedo of snow I: pure snow, J. Atmos. Sci., 37: 2734-2745.

Table 1. Comparison of co-albedos ($1 - \Omega$) from the parameterized equation(P) with the Mie results interpolated from Wiscombe and Warren (1980) (WWI). The ice absorption coefficients are from WWI.

r(μm)	Model	λ(μm)			
		0.4	1.1	1.3	2.0
50.0	P	1.785×10^{-6}	1.09×10^{-3}	4.91×10^{-3}	2.577×10^{-1}
	WWI	1.8×10^{-6}	1.1×10^{-3}	5.0×10^{-3}	2.59×10^{-1}
200.0	P	7.147×10^{-6}	4.35×10^{-3}	1.934×10^{-2}	4.482×10^{-1}
	WWI	7.0×10^{-6}	4.4×10^{-3}	1.9×10^{-2}	4.48×10^{-1}
1000.0	P	3.573×10^{-5}	2.135×10^{-2}	8.901×10^{-2}	4.67×10^{-1}
	WWI	3.3×10^{-5}	2.1×10^{-2}	9.0×10^{-2}	4.69×10^{-1}

Table 2. Comparison of asymmetry parameters (G) from the parameterized equation (P) with the Mie results interpolated from Wiscombe and Warren (1980) (WWI). The ice absorption coefficients are from WWI.

r(μm)	Model	λ(μm) 0.4	1.1	1.3	2.0
50.0	P	0.886	0.886	0.887	0.933
	WWI	0.886	0.887	0.890	0.934
200.0	P	0.886	0.887	0.890	0.970
	WWI	0.887	0.895	0.900	0.972
1000.0	P	0.886	0.890	0.902	0.972
	WWI	0.889	0.90	0.912	0.977

Table 3. Observed and model physical parameters for Figures 3 and 4.

Figure	Observed Parameters		Model Parameters	
	Grain Radius (mm)	Impurity (ppmw)	Grain Radius (mm)	Impurity (ppmw); soot
3A	0.025 to 0.05*	†	0.07	0.30
3B	0.10 to 0.15	†	0.20	0.30
3C	0.38 to 1.0*	<500 (dust)	2.2	0.055
4**	0.13 to 0.25* (x < 30 mm)	†	1.0 (x ≤ 30 mm)	0.03 (x ≤ 30 mm)
	0.25 to 0.50* (x > 30 mm)		2.0 (x > 30 mm)	0.05 (x > 30 mm)

* smallest dimension of typical particle

** density (kg m^{-3}) - 350 for x ≤ 30 mm, 450 for x > 30 mm

† Not measured

FIGURE CAPTIONS

Fig. 1: Schematic illustration of the albedo model. Δx is layer thickness, ρ is density, r is grain radius, and S is the amount of soot in parts per million by weight. The subscripts are layer indices. F is the spectral incident flux and A is the spectral albedo of the snow-soil system.

Fig. 2: Spectral albedo of wet clay soils.

Fig. 3: Comparison with observed albedo for deep impure snowpacks. The dotted lines are for pure and solid lines are for soot contaminated snow. The physical properties of snow are given in Table 3.

Fig. 4: Comparison with observed albedos for a two-layer snowpack. The dotted line is for pure snow in the top layer, the sub-layer being soot contaminated.

Fig. 5: Illustration of the effect of soot contamination for 20 mm thick snowpacks. (a) fairly new snow, (b) fairly old snow. The curves are labeled with the amount of soot (0.0, 0.05 ppmw).

Fig. 6: Spectral albedos from 400 to 1000 nm of a shallow snowpack for several discrete values of soot concentration. Spectral curves are labeled with the soot content (ppmw). This figure illustrates that soot first increases the albedos (left) and then reduces it (right).

Fig. 7: The aircraft albedo data (o) and the parametric equation (dashed line) used for interfing the fractional snow covered area. See text for the meaning of symbols.

Fig: 8: The relative albedos (i.e., the albedos normalized to 100 percent at the snow thickness of 650 mm) for the NOAA-2 data (o). The dashed line is from Eqn. 28.

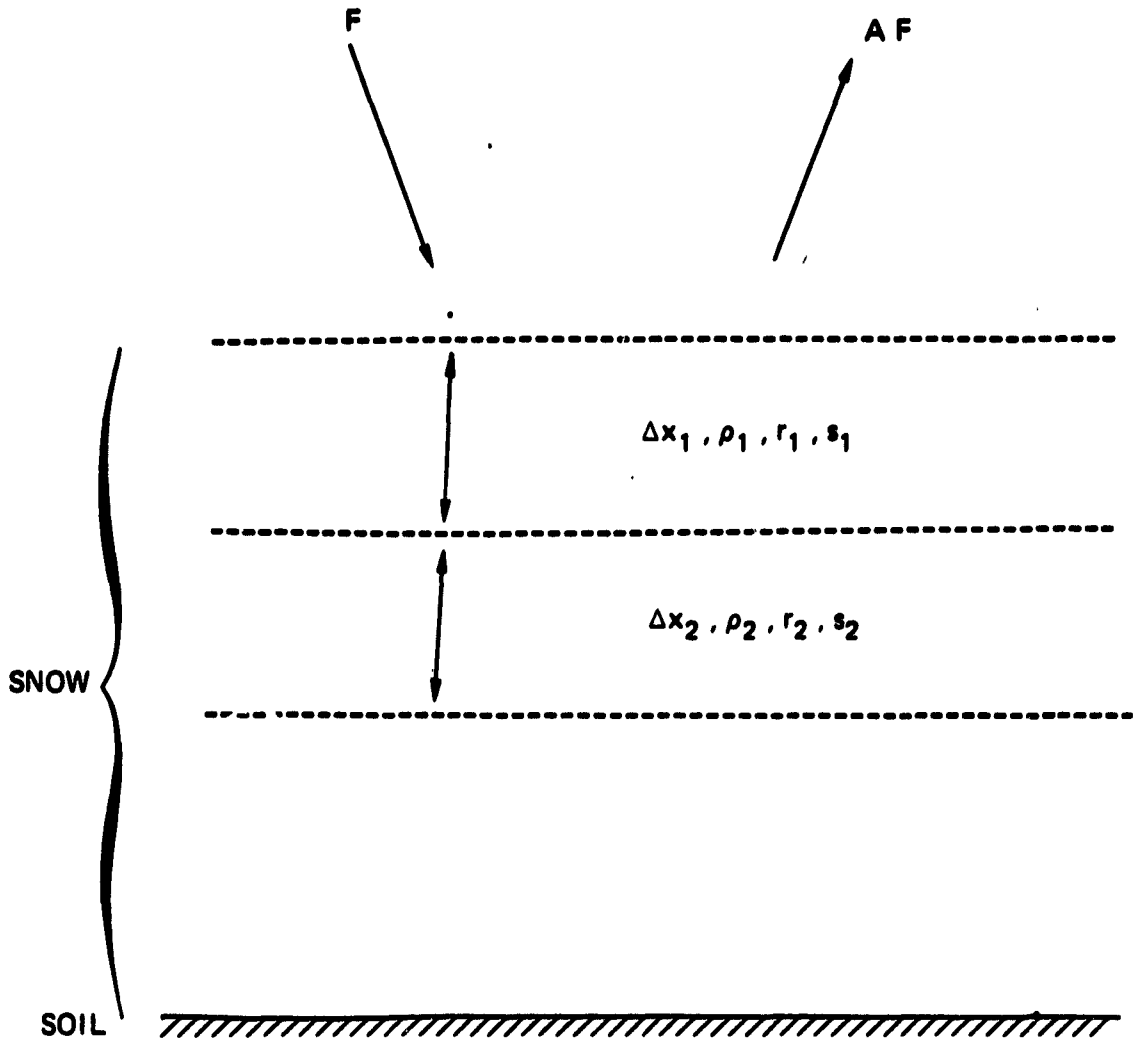

Figure 1. Schematic illustration of the albedo model. Δx is layer thickness, ρ is density, r is grain radius, and s is the amount of soot in parts per million by weight. The subscripts are layer indices. F is the spectral incident flux and A is the spectral albedo of the snow-soil system.

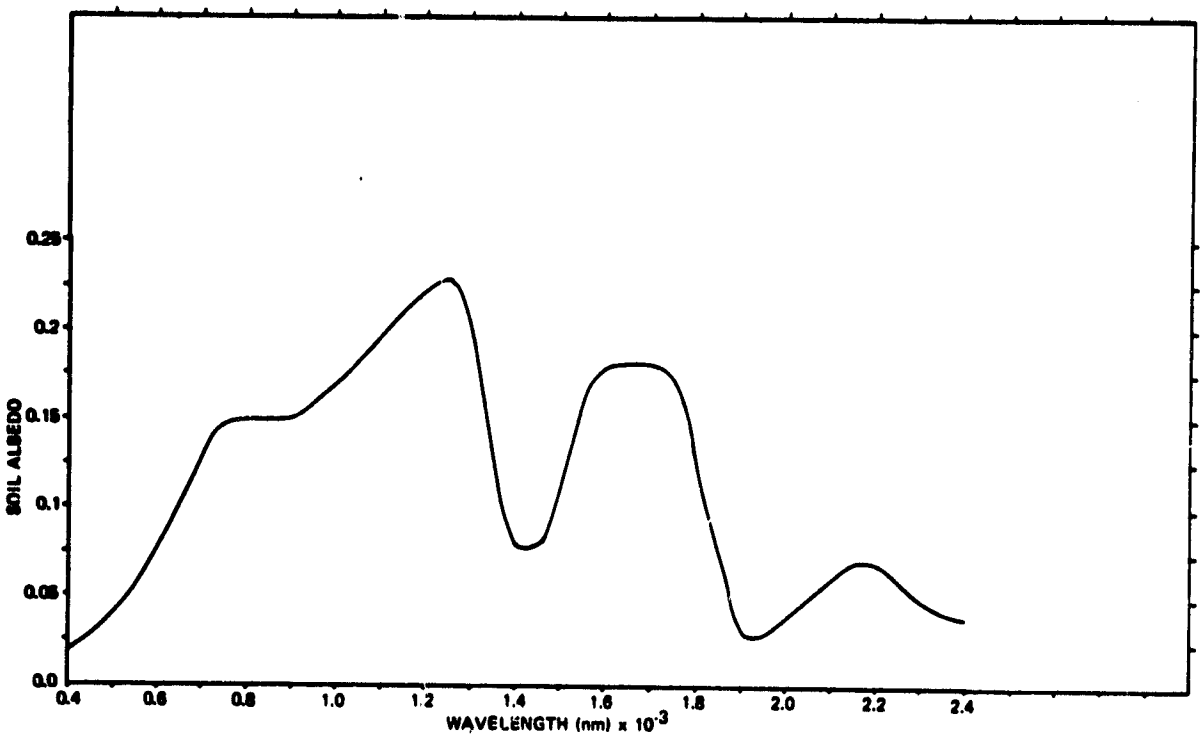

Figure 2. Spectral albedo of wet clay soils. (Lulla, 1980)

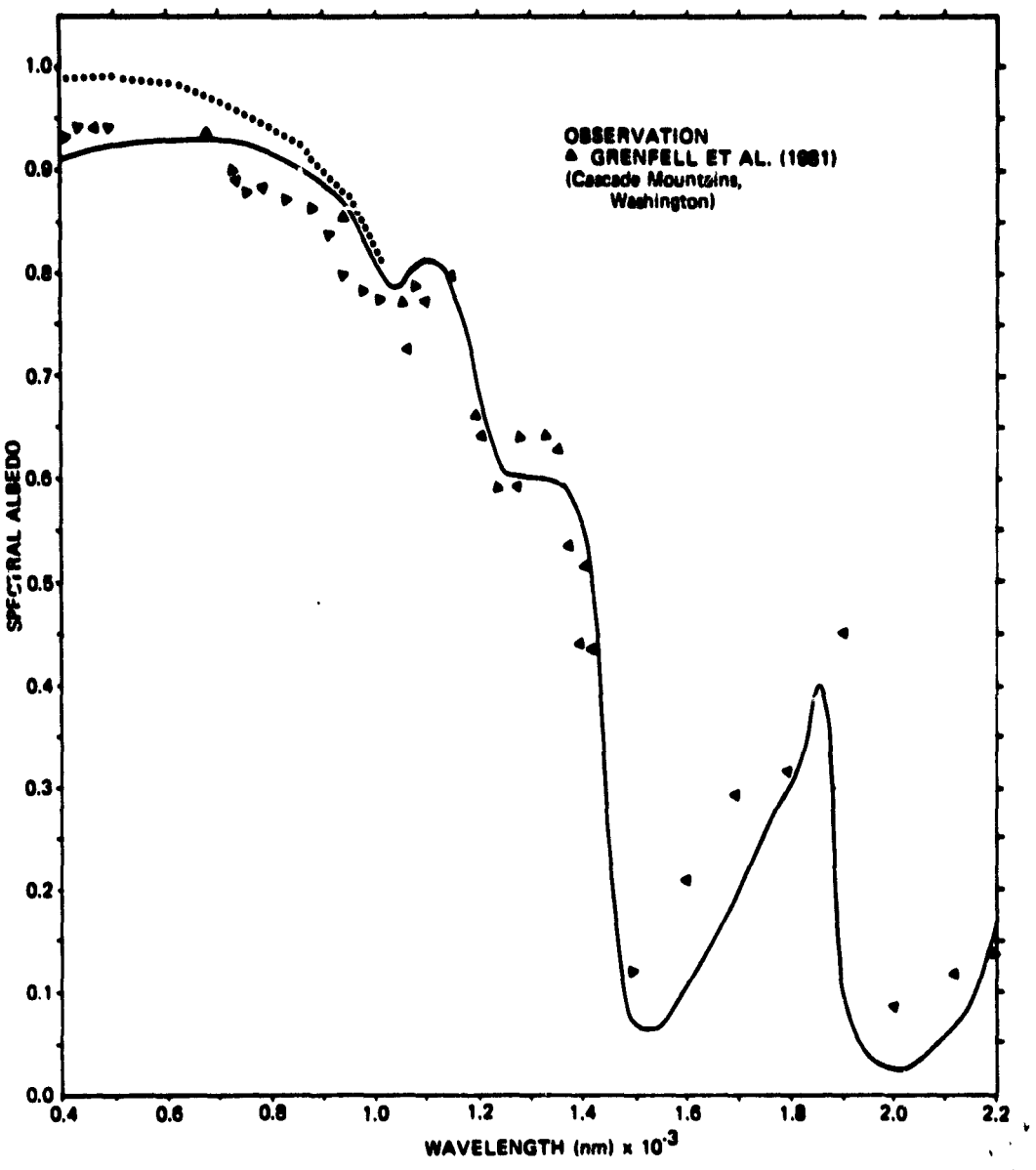

Figure 3a. Comparison with observed albedo for deep impure snowpacks. The dotted lines are for pure and solid lines are for soot contaminated snow. The physical properties of snow are given in Table 3.

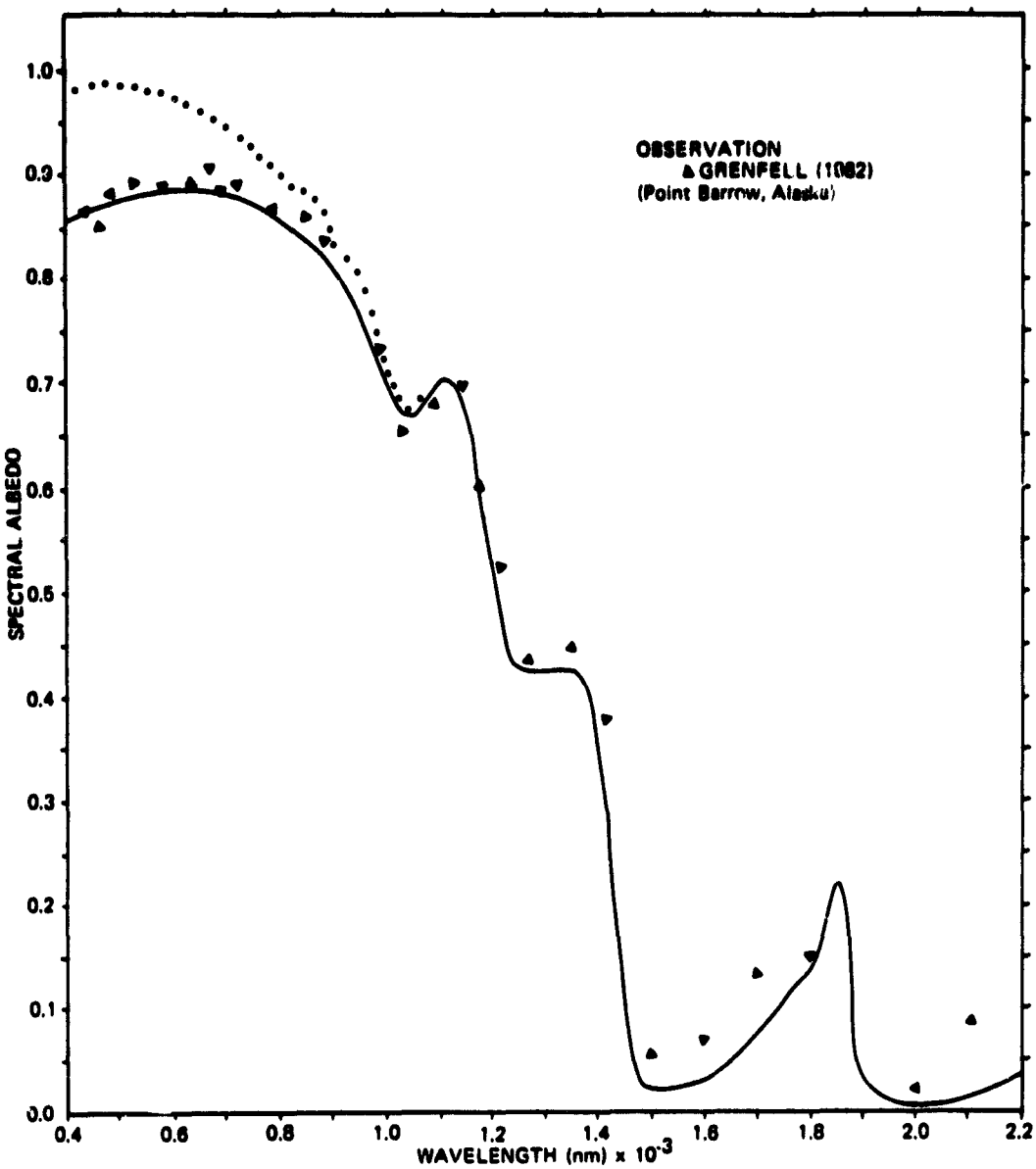

Figure 3b. Comparison with observed albedo for deep impure snowpacks. The dotted lines are for pure and solid lines are for soot contaminated snow. The physical properties of snow are given in Table 3.

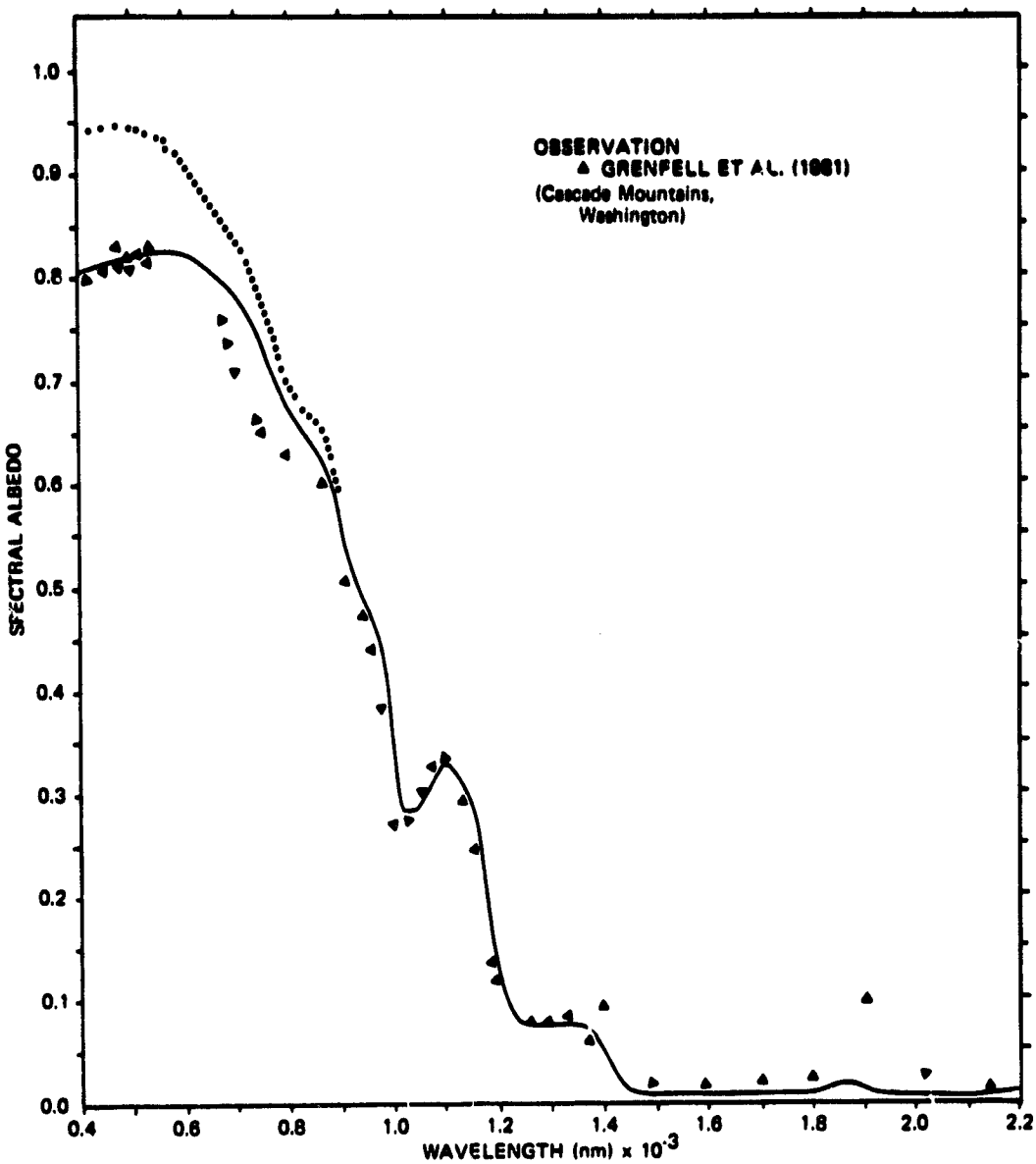

Figure 3c. Comparison with observed albedo for deep impure snowpacks. The dotted lines are for pure and solid lines are for soot contaminated snow. The physical properties of snow are given in Table 3.

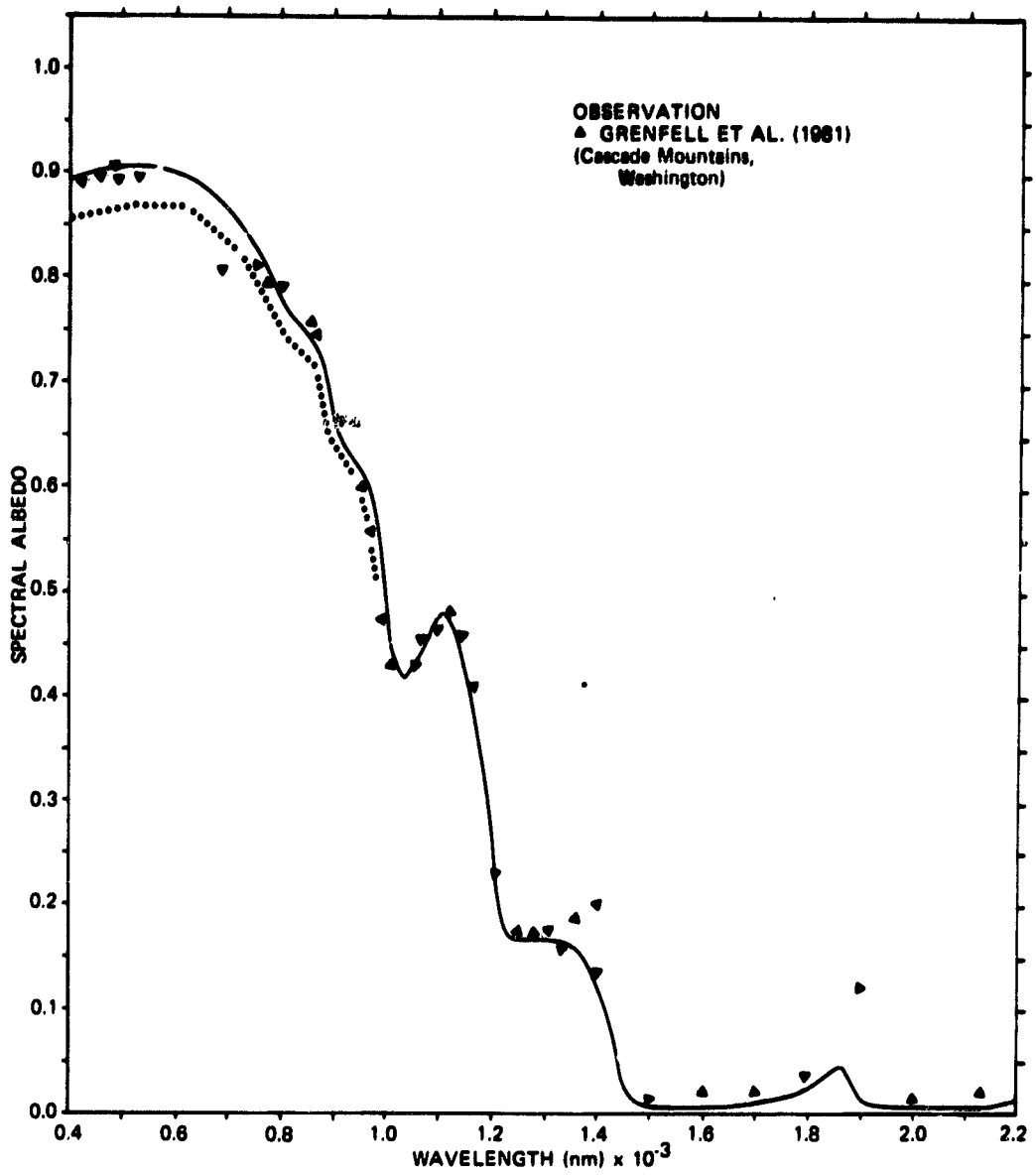

Figure 4. Comparison with observed albedos for a two-layer snowpack. The dotted line is for pure snow in the top layer, the sub-layer being soot contaminated.

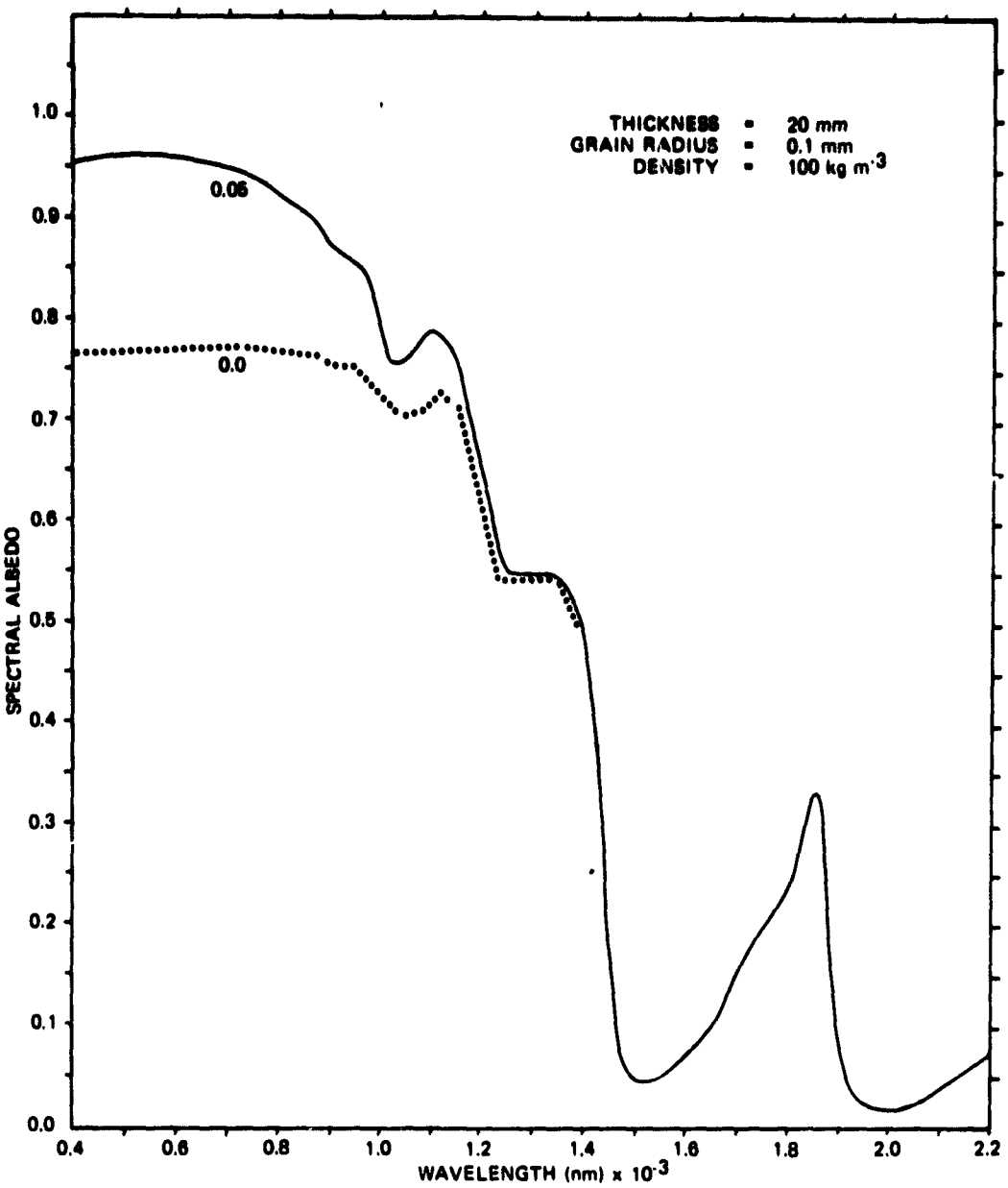

Figure 5a. Illustration of the effect of soot contamination for 20 mm thick snowpacks, fairly new snow. The curves are labeled with the amount of soot (0.0, 0.05 ppmw).

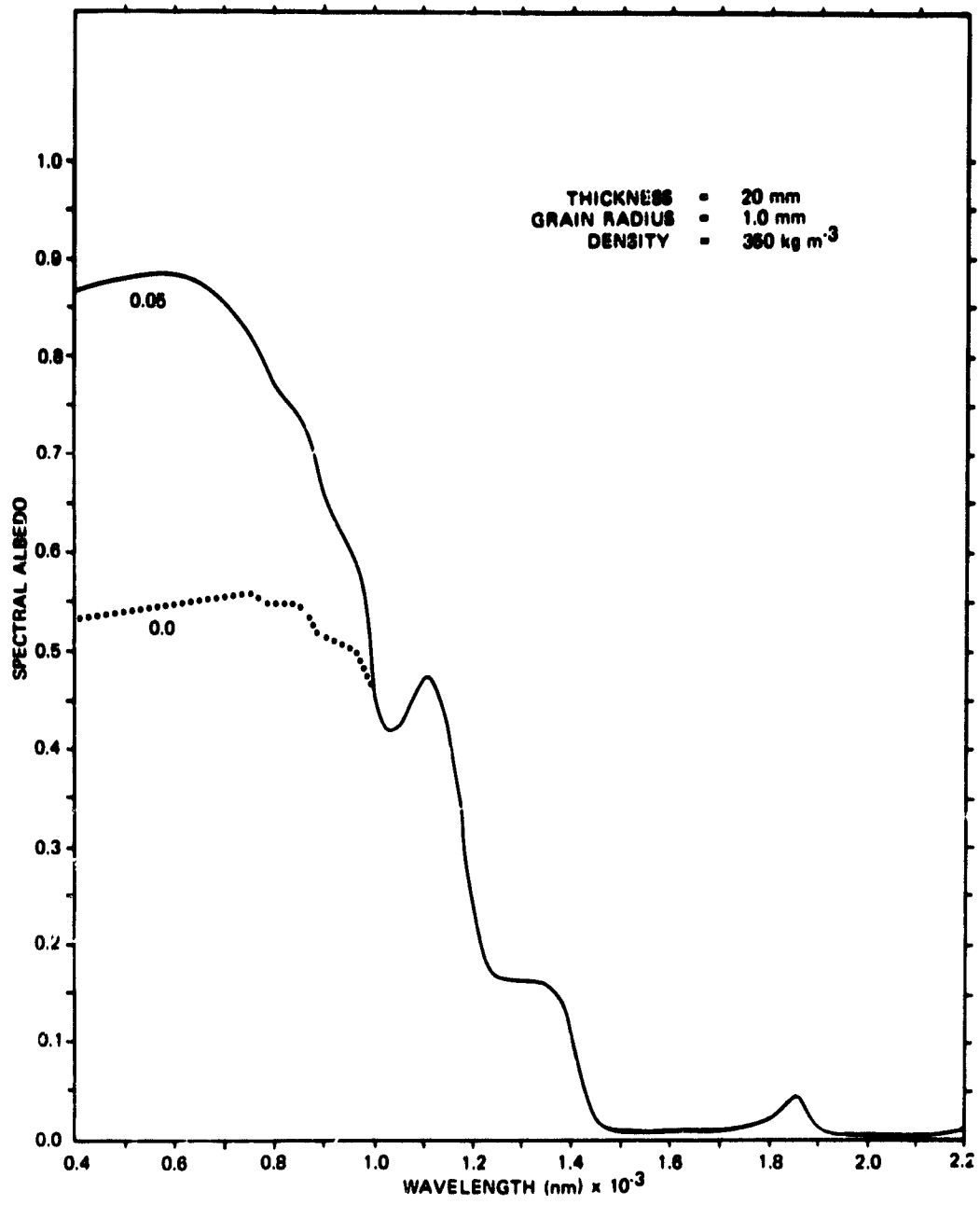

Figure 5b. Illustration of the effect of soot contamination for 20 mm thick snowpacks, fairly old snow. The curves are labeled with the amount of soot (0.0, 0.05 ppmw).

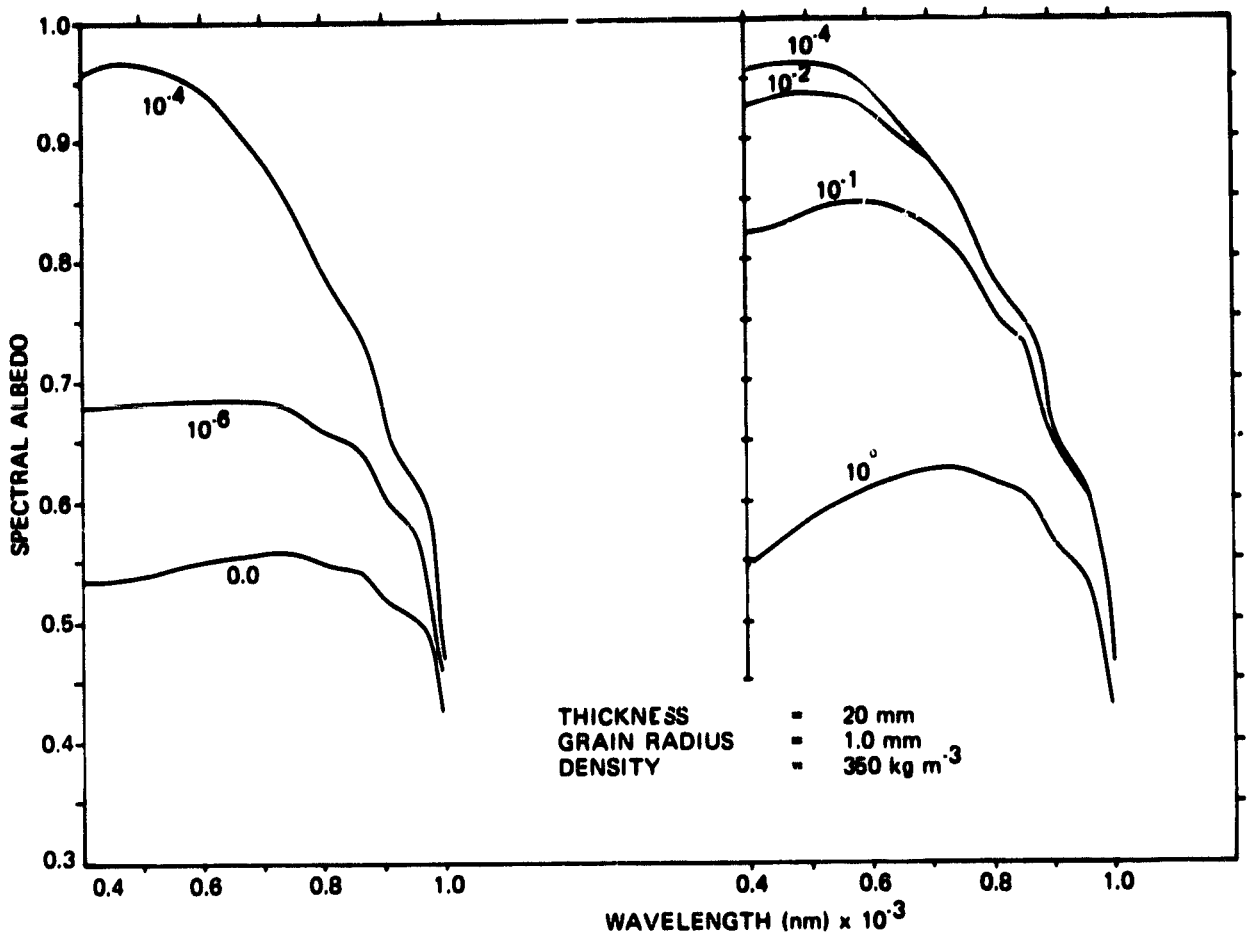

Figure 6. Spectral albedos from 400 to 1000 nm of a shallow snowpack for several discrete values of soot concentration. Spectral curves are labeled with the soot content (ppmw). This figure illustrates that soot first increases the albedos (left) and then reduces it (right).

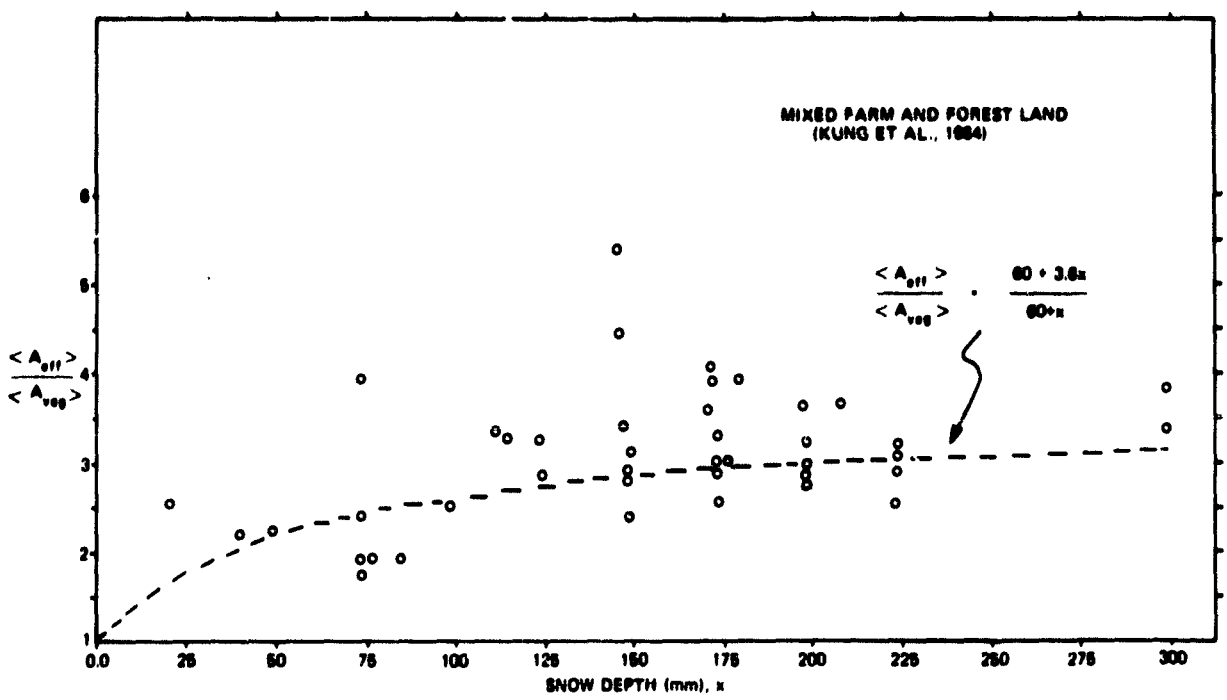

Figure 7. The aircraft albedo data (o) and the parametric equation (dashed line) used for inferring the fractional snow covered are See text for the meaning of symbols.

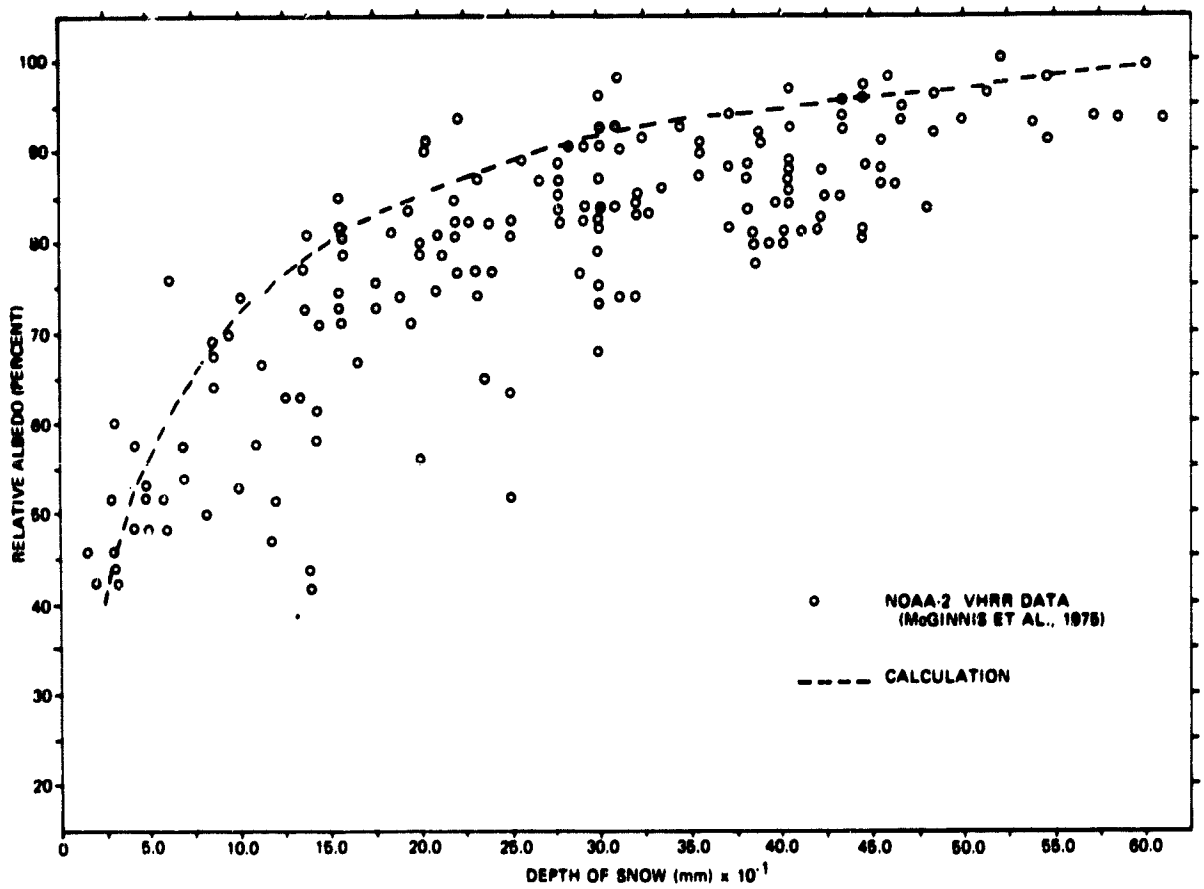

Figure 8. The relative albedos (i.e., the albedos normalized to 100 percent at the snow thickness of 650 mm) for the NOAA-2 data (o). The dashed line is from Eqn. 28.